

# WEAR RESISTANT AMORPHOUS AND NANOCOMPOSITE STEEL COATINGS

D.J. Branagan, W.D. Swank, D.C. Haggard, J.R. Fincke  
Idaho National Engineering and Environmental Laboratory

## ABSTRACT

In this paper, amorphous and nanocomposite thermally deposited steel coatings have been formed by using both plasma and high velocity oxy-fuel (HVOF) spraying techniques. This was accomplished by developing a specialized iron based composition with a low critical cooling rate ( $\approx 10^4$  K/s) for metallic glass formation, processing the alloy by inert gas atomization to form micron sized amorphous spherical powders, and then spraying the classified powder to form coatings. A primarily amorphous structure was formed in the as-sprayed coatings independent of coating thickness. After heat treating above the crystallization temperature ( $568^\circ\text{C}$ ), the structure of the coatings self-assembled (i.e. devitrified) into a multiphase nanocomposite microstructure with 75-125 nm grains containing a distribution of 20 nm second phase grain boundary precipitates. Vickers microhardness testing revealed that the amorphous coatings were very hard (10.2 to 10.7 GPa), with further increases in hardness after devitrification (11.4 to 12.8 GPa). The wear characteristics of the amorphous and nanocomposite coatings were determined using both two body pin on disk and three body rubber wheel wet slurry sand tests. The results indicate that the amorphous and nanocomposite steel coatings are candidates for a wide variety of wear resistant applications.

## INTRODUCTION

Recently, a significant effort has been directed at developing nanoscale structures in coatings produced by thermal deposition techniques. Two approaches have been commonly used; the first approach is to start with heavily deformed mechanically processed micron sized powder that has a nanoscale structure<sup>1-7</sup> and the second approach relies on directly spraying either nano-size powders<sup>8</sup> or nano-powder precursors<sup>9-11</sup>. Both approaches rely on maintaining the existing nanoscale structure during spraying and subsequent impact on the substrate. In the spraying of mechanically processed micron sized powders with nanoscale structures, complete melting of the powder must be avoided<sup>5,7</sup> and the elevated temperature exposure of the particles must be sufficiently short so that grain growth and coarsening does not occur to a significant extent<sup>6</sup> or the desired nanostructure will be lost. The second approach, the direct spraying of nanophase powder has its own set of limitations associated with the process. The primary issue is the introduction of nano-sized powders into the high velocity thermal spray jet and their impingement on the substrate. Nano-sized powders tend to agglomerate, resulting in plugged particle feed lines and the extremely small particles do not readily penetrate the jet, and hence are not exposed to the temperatures required for melting. The other issue is that nano-sized powders readily follow the gas streamlines and do not impinge on the substrate to be coated,<sup>9</sup> which makes it difficult to form a coating with high deposition efficiency. This problem can be circumvented by agglomeration of nano-sized particles with a binder, especially in cases where the binder is a lower melting point material such as Co used in the Co-WC cermet system.<sup>9</sup> Unfortunately this approach is useful for only a limited number of material systems. Another methodology which has been used is to introduce the material as a liquid or gaseous precursor, which reacts in-flight to form nano-sized particles.<sup>10-12</sup> This approach is promising, however it

suffers from low deposition efficiency, as the in-flight synthesized powder tends to follow the gas flow streamlines when performed at atmospheric pressure. This limitation can be overcome by operating at extremely high velocity and reduced pressure.<sup>12</sup> Under these conditions, the aerodynamic drag force on the particle is reduced and the rate of impact on the substrate greatly increased. The disadvantage is the increased cost and complication of operating at reduced pressure in a controlled atmosphere environment. The deposition of coatings from liquid or gaseous precursors has been demonstrated for a limited number of oxide and carbide systems and is generally not applicable to the formation of metallic coatings.

Many attempts at developing nanoscale structured coatings have been conducted using high-velocity oxy-fuel thermal spray devices (HVOF). Because of the high particle kinetic energy available in the HVOF thermal spray process partially molten or “soft” particles are capable of forming acceptable coatings without the requirement of complete particle melting. The avoidance of complete particle melting and the rapid quenching of the particle upon impact on the substrate are advantageous to the retention of the starting nanostructure. Still excessive grain growth is an issue. The mechanically alloyed powder contains a high amount of internal stress, which results in rapid coarsening through recovery and recrystallization mechanisms and the nanopowder contains an extremely high amount of external surface area that rapidly sinters into coarse structures. Rapid coarsening in both of these approaches to develop nanoscale structures occurs at temperatures below 0.5 of the melting temperature.

In this paper, a different approach that is capable of achieving nanoscale microstructures in metallic coatings by post processing the coating through a solid/solid state transformation is demonstrated. This general methodology involves designing alloys that have low critical cooling rates for metallic glass formation, that enables the formation of amorphous coatings when thermally deposited. The amorphous coatings, while exhibiting interesting properties, can be heated up above their crystallization temperature to initiate devitrification. Since the driving force for the transformation is extremely high and the diffusion rate in the solid state, at the transformation temperature, is very low, an extremely high nucleation frequency results. There is limited time for growth before impingement between neighboring grains resulting in the formation of nanoscale microstructures. By altering the composition, nanoscale composite microstructures can be formed directly with dispersions of small (5-10 nm) precipitates that form at the grain and phase boundaries. This results in microstructures which are strongly pinned and which resist grain growth to high fractions ( $\approx 0.8$ ) of the melting temperature. In this study, both HVOF and plasma thermal spray deposition processes were used to demonstrate the ability to produce amorphous and nanocomposite coatings out of a specially formulated steel composition.

## EXPERIMENTAL PROCEDURE

The steel alloy composition ( $\text{Fe}_{63}\text{Cr}_8\text{Mo}_2\text{B}_{17}\text{C}_5\text{Si}_1\text{Al}_4$ ) studied in this paper was designed using basic principles of metallic glass formation resulting in a low ( $10^4$  K/s) critical cooling rate for metallic glass formation. Two methods were used to form the alloys investigated. For the powders utilized in plasma spraying, high purity elements ( $> 99.5$  wt%) were alloyed insitu via RF melting prior to atomization. For the powders utilized in HVOF spraying, high purity elements ( $>99.5$  wt%) were induction melted and vacuum cast into prealloyed ingots which were subsequently used for feedstock for atomization. The latter method resulted in more uniform melting, lower melt reactivities, and fewer atomization failures. Inert gas atomization (IGA) was

done on a lab built, close coupled, annular feed gas atomization system. Helium gas with a pressure of 400 psi was used to both aspirate and break up the liquid melt stream into individual powder particles that solidify during freefall. Spherical powder particles with few satellites or pores were produced with a gaussian powder size distribution from submicron to  $\approx 150 \mu\text{m}$ . The powder for thermal spray deposition was sieved below  $50 \mu\text{m}$  and then air classified to remove the fines. Heat treating of the coatings was performed in a radiative vacuum furnace at  $10^{-6}$  torr. Differential thermal analysis (DTA) and Differential Scanning Calorimetry (DSC) of both the powder and the spray coatings was performed in a Perkin Elmer DTA-7 from  $30^\circ\text{C}$  to  $1375^\circ\text{C}$  at a heating rate of  $10^\circ\text{C}/\text{min}$  in a  $50 \text{ ml/s}$  flowrate of UHP Ar. Scanning electron microscopy (SEM) was done using a Philips XL30 ESEM. X-ray diffraction was carried after incorporation of a silicon standard using a Bruker X-ray Diffractometer with filtered  $\text{Cu-K}_\alpha$  radiation and a LiF monochromometer. Analysis of the experimental X-ray patterns was done by Rietveld analysis using SIROQUANT V 2.0 software. Vickers microhardness measurements were done with a  $100 \text{ g}$  load on metallographically mounted cross sections of 75 to 100 particles or thermally deposited coatings using a Leco M-400-H1 System. Before spraying, the substrates were degreased, grit blasted using  $\text{Al}_2\text{O}_3$ , and cleaned in ethanol. Plasma spraying was accomplished using a Praxair SG-100 plasma arc spray gun in a vacuum chamber which was evacuated and then backfilled with 300 Torr Argon. The gun was rastered across the samples in a horizontal stroke with  $3 \text{ mm}$  vertical spacing between subsequent passes. During spraying the substrates and coatings were cooled by argon jets mounted on the gun with a pressure of  $250 \text{ p.s.i.}$  directed at the substrate. HVOF spraying was done using a Tafa / Praxair JP-5000 gun with a  $4''$  barrel operating at an equivalence ratio of  $0.8$  and a chamber pressure of  $\approx 552 \text{ kPa}$ . The gun rastered across the sample with a  $5 \text{ mm}$  spacing and a  $7 \text{ second}$  cooling time between subsequent layers. Adhesion testing was done per ASTM C633 using Magna-Tec Industrial Strength Adhesive M777 epoxy with a crosshead speed of  $0.05 \text{ in}/\text{min}$ . Two body abrasion tests were conducted via pin on disk testing per ASTM G99 on a Falex-ISC Pin on Disk machine with no lubrication using a  $\frac{1}{2}''$   $\text{Si}_3\text{N}_4$  ball rotated at a test speed of  $97 \text{ rpm}$  with a test radius of  $10.4 \text{ mm}$ . Three body wear tests via wet sand rubber wheel testing were done in accordance with ASTM G105 using AFS Testing Sand 50-70.

## RESULTS and DISCUSSION

### Powder Production and Properties

The powder size distribution determined by sieving is shown in Figure 1. The powder that is produced typically exhibits a gaussian distribution in particle size with a cumulative weight percent average of  $\approx 25 \mu\text{m}$ . The fine powder particles, that cool the fastest, exhibit an X-ray diffraction pattern typical of an amorphous structure with a broad amorphous hump and lack of Bragg diffraction peaks (Figure 2). As the particle size is increased, the cooling rate decreases, and the amount of crystallinity increases. The amount of glass as a function of powder particle size can be found from DSC by assuming that the smallest particles are 100% glass and then comparing the ratio of crystallization enthalpies of each size fraction to that of the smallest particles. The results show that a significant fraction of the less than  $50 \mu\text{m}$  particles are amorphous while particles greater than  $75 \mu\text{m}$  are crystalline (Figure 1). In Figure 3, backscattered electron micrographs indicate small particles ( $< 20 \mu\text{m}$ ) have an absence of structure while larger powder particles ( $50 - 75 \mu\text{m}$ ) exhibit a primarily crystalline structure with pockets of uncrystallized glass. When heating above the crystallization onset temperature

(568°C), the glass devitrifies via a solid/solid transformation into a nanoscale composite structure typically consisting of 50 to 75 nm grains pinned by extremely fine 5-10 nm carbide and boride second phases. The devitrified structure of the amorphous particles has been described elsewhere.<sup>13</sup>

### **Thermal Spray Coatings and Properties**

To facilitate thermal spray deposition, the atomized powder was sieved to remove particles greater than 50  $\mu\text{m}$  diameter and was air classified to remove the fine particles less than 10  $\mu\text{m}$  in diameter. A typical powder size distribution of the classified powder is shown in Figure 4. While this powder could easily be plasma sprayed, the remaining small fraction of fine particles caused some barrel loading problems during HVOF, which was corrected by using an additional sieving step to further reduce the fines. Plasma spraying was done onto 4" by 4" 301 stainless steel substrates to perform two body wear tests. HVOF deposition was done onto 4340 alloy steel, 13-8 precipitation hardenable stainless steel, and 7075 aluminum in a wide variety of shapes in order to perform adhesion, three body wear and physical metallurgical tests (Figure 5). The initial plasma and HVOF deposited samples exhibited porosity determined from metallographic software to be 3.0% and 3.4% (Figure 6A) respectively. Optimization of the HVOF processing parameters resulted in the formation of high density (>99.9% dense) coatings (Figure 6B).

Both the as-deposited HVOF and plasma sprayed coatings were found to be primarily amorphous from X-ray diffraction with the scans exhibiting a broad amorphous hump with the presence of very low intensity peaks. X-ray diffraction scans were done on the free surfaces of the HVOF coating (Figure 7) but the substrate surface could not be analyzed since the coating or pieces of the coating could not be removed from the substrate. To produce a free standing coating, plasma spraying was used to build up ( $\approx 30$  layers) a thick 1650  $\mu\text{m}$  deposit which delaminated from the substrate during cooling from thermal stresses. X-ray diffraction was performed on both the free surface and substrate surface (Figure 8a and 8b). Since little difference is found from the substrate to the free surface in this extreme case, this suggests that the amorphous characteristics are maintained independent of the number of layers. On both Figures 7 and 8, peaks above the amorphous background can be seen indicating crystalline phases in the glass. Analysis of these peaks reveal that they are from the 23/6 type phases identified in Table 1 which indicates that these phases form first during crystallization. A more detailed thermal analysis of the coating was performed to determine crystallinity. The DTA curves showing the glass to crystalline transformation for the HVOF, plasma, and atomized feedstock powder are given in Figure 9. From DSC measurements, the enthalpy of the glass to crystalline transformation and the corresponding percent glass was found to be  $-58.4$  J/g (46% glass),  $-52.6$  J/g (41% glass), and  $-109.7$  J/g (86% glass) for the starting powder, HVOF coating, and plasma sprayed coating respectively. The fact that the HVOF coating contains less than 50% glass is surprising from the corresponding X-ray diffraction diagram which indicates that the crystalline fraction which is present in the glass is nanoscale.

After devitrification at 750°C for 1 hr, the microstructure of the HVOF fabricated sample was studied using both X-ray diffraction and TEM. Rietveld refinement was performed on the experimental X-ray diffraction data with very good results (total Chi-squared = 2.4) and with all of the peaks identified (Figure 10). A summary of the phases found and their corresponding

structural information and lattice parameters are given in Table 1. From TEM, the structure of the coating was found to be nanoscale with grains from 75 to 125 nm with 20 nm second phase precipitates at the grain boundaries (Figure 11).

The adhesion strength of the HVOF sprayed samples was tested on a variety of common metal substrates including 7075 aluminum, 13-8 precipitation hardenable stainless steel, and 4340 alloy steel substrates. Three tests were done on each substrate material with failure generally observed from 4000 to 5000 lb/in<sup>2</sup>. Inspection of the failure surface showed that, in all cases, the failure was in the epoxy and the steel coating did not fracture or pull away from the substrate. Thus, the adhesion strength of the coating to the substrate and the cohesive strength of the coating could not be determined since these strengths are higher (i.e. > 5000 lb/in<sup>2</sup>) than the strength of the Magnatec adhesive.

### **Hardness / Wear Characteristics**

The hardness of the as-sprayed and heat treated coatings were measured using Vickers and the average of 10 measurements are reported with their corresponding standard deviation (S). The hardness of the as-sprayed plasma sprayed sample was 10.7 GPa (S=0.32) and after heat treating at 800°C for 1 hour this increased to 12.8 GPa (S=0.76). The hardness of the as-sprayed HVOF sample was 10.2 GPa (S=0.85) and after a 750°C for 1 hour heat treatment that increased to 11.4 GPa (S=0.98).

Tribology testing for two body abrasive wear was performed on both the as-sprayed and heat treated (800°C 1 hr) plasma deposited coatings. The profile curve of the wear groove of the as-sprayed sample using the Si<sub>3</sub>N<sub>4</sub> pin can be seen in Figure 12. Instead of the expected wear groove in the steel coating, a hill of material was found which was deposited from the pin. Post examination of the Si<sub>3</sub>N<sub>4</sub> pin revealed that it exhibited a ball scar of diameter 0.853 mm. A similar result showing no evidence for wear of the coating was found in the heat treated sample. These results were surprising due to the high hardness (15.4 GPa) of the Si<sub>3</sub>N<sub>4</sub> ball material which is the hardest commercially available pin material. During the tests, the coefficients of friction were measured and the data is shown in Figure 13 for the as-sprayed coating. The coefficient of static friction for both the as-sprayed and heat treated steel coating /Si<sub>3</sub>N<sub>4</sub> ball couple was found to be 0.22. The coefficient of sliding friction for the steel coating could not be measured due to Si<sub>3</sub>N<sub>4</sub> deposition from the pin.

Three body wet sand rubber wheel wear tests were performed on both the as-sprayed and heat treated (750°C 1 hr) unpolished HVOF deposited coatings in comparison with a 1090N steel plate and a HVOV deposited WC cemented carbide coating (Table 2). The as-sprayed steel sample exhibited a weight loss similar to the 1090N steel. After heat treating the wear characteristics of the nanocomposite steel improved dramatically with a reduction by a factor of 4 in weight loss. The WC-cemented carbide sample exhibited the best three body wear resistance of all the alloys studied in this test.

Significant differences were observed in the coatings produced by two different thermal spray methods which were employed. Initially coatings were fabricated using thermal plasma spraying. HVOF thermal spraying was investigated because of its ability to produce high density coatings with lower residual stress and improved metallurgical bonding to the substrate. The

HVOF spray parameters were optimized by metallographic examination to minimize porosity, resulting in nearly fully dense coatings. Conventional wisdom suggests that the higher density coatings should result in higher hardness. However, higher hardness was obtained in the plasma sprayed coatings in spite of their higher porosity, indicating differences in their microstructures.

The plasma deposited coating was found to contain a high percent of glass (86%) in the as-sprayed condition which was much higher than the starting powder (46%) and the HVOF coating (41%). The only way to increase the amount of glass, is to go through a remelting to the liquid state followed by quenching into the glass state. Since the starting composition is the same, the difference in the glassy fraction is related to the mechanics of the two spray processes. In the plasma gun, the plasma temperature is very high ( $\approx 12,000$  K) and the velocity which the particles are sprayed is moderate (200 m/s). In the HVOF process, the flame temperature is much lower ( $\approx 3000^\circ\text{C}$ ) while the velocity of the powder particles is much higher (800 m/s). Thus, in the plasma gun, the individual powder particles experience a significant increase in residence time with exposure to much higher temperatures. Thus, the powder particles were completely remelted in the plasma gun and then were rapidly solidified and quenched on the substrate forming a glass. The similar values of glass fraction found in the starting feedstock powder and HVOF coatings suggests that the particles did not remelt to a significant extent which explains the higher percentage of glassy phase in the plasma sprayed coatings. Note that the HVOF process can be further optimized to maximize the remelting while still producing high density coatings.

After heat treating, the glass fraction in the coating devitrifies into a nanoscale composite structure. The bulk of the crystalline fraction in the as-sprayed coatings probably formed initially in the feedstock powder through nucleation and growth processes in the liquid during atomization. These regions which did not undergo a glass devitrification solid/solid state transformation, while submicron due to the high undercooling, are still coarser than the devitrified regions. Thus, the hardness measured in the heat treated coating, will be dependant on both the fraction of precursor glass in the coating and the density of the coating, neither of which have been optimized in this study.

The hardness levels (11.4 to 12.8 GPa) measured in the devitrified nanocomposite steel coatings are significantly higher than found in conventional steels which attain a maximum hardness of 9.2 GPa ( $R_c=68$ ). This result cannot be attributed to the hardness of any particular phase since the phases identified in the X-ray diffraction scans are not particularly hard but instead from the development of the nanoscale microstructure. Analogous to the bulk scale, it can be expected that the extremely large volume fraction of 2-d interfacial grain and phase boundaries will create barriers preventing dislocation motion resulting in increases in strength and hardness. The exact mechanism of strengthening is unclear but recent studies suggest that nanocrystalline grains cannot support dislocation pileups<sup>14</sup> resulting in dislocation mediated plasticity being inhibited. This significantly increases the critical stress levels needed to initiate plasticity.<sup>15</sup>

Due to the high hardness, the amorphous and nanocomposite coatings experienced good wear characteristics. No wear was found in the two-body abrasion tests in the as-sprayed or heat treated plasma coatings. This was surprising since the  $\text{Si}_3\text{N}_4$  pin was much harder than both the

as-sprayed and heat treated coatings. While the reason for this is not clear, it could be due to the difference in the nature of the bonding between the steel and the silicon nitride; i.e. metallic vs covalent bonds. In the three-body wet slurry rubber wheel wear tests, the as-sprayed steel coatings exhibited a significant amount of wear which was reduced by a factor of four in the heat treated nanocomposite coating. However, the three body abrasion resistance of the heat treated steel was not as good as the commercially mature WC-cemented carbide coatings. These results can be interpreted based on the hardness of the substrates. The WC cemented carbide coating was the hardest (12.8 GPa) of the coatings tested and exhibited the best wear resistance. Generally, when the ratio of the hardness of the abrasive divided by the hardness of the substrate approaches or exceeds unity then the abrasive wear resistance increases significantly.<sup>16</sup>

## CONCLUSIONS

As a result of these studies, we have shown that steel coatings with a metallic glass structure could be formed by both plasma and HVOF spraying. Additionally, in contrast to the existing body of work in metallic glasses, we showed that the development of a metallic glass state is possible by spraying in air without a cover gas. This is significant since previous work on Zr-based glasses, which are very sensitive to oxygen, has indicated that glasses must be processed in high purity environments.<sup>17</sup> The results indicate that thick amorphous coatings can be developed independent of layer thickness during spraying, since subsequent layers did not promote crystallization of the underlying layers. The only limitations in the thickness of the amorphous coatings appear to be thermal stress which limits the coating to  $\approx 1500 \mu\text{m}$ . Additionally, we have shown that highly stable nanocomposite structures could be developed in the coatings after a devitrification heat treatment.

Studies of the properties of these coatings have revealed that high hardness, superior to that found in conventional steels could be developed in both the as-sprayed amorphous (10.2 to 10.7 GPa) and devitrified nanocomposite (11.4 to 12.8 GPa) steel coatings. Using HVOF deposition, the adhesion strength of the coatings were found to be excellent for a wide variety of metallic substrates. Two body pin on disk tests using a very hard  $\text{Si}_3\text{N}_4$  pin showed that the amorphous and nanocomposite steel coatings exhibit exceptional two body abrasion resistance. Good wear resistance was obtained in the three body slurry abrasion tests but the wear resistance was not as good as the commercially mature WC-cemented carbide coatings.

Analysis of the results reveal the pathway to achieving higher hardness and improved three body wear resistance. A key factor is to produce high density coatings which ideally contain 100% glass, which can be subsequently transformed into nanocomposite structures. This data suggests that this can be achieved by a combination of two approaches. The critical cooling rate of the starting alloy can be reduced so that completely amorphous atomized powders are produced in the feedstock powder range. The spray conditions in HVOF can also be optimized to increase the residence time and/or the gas reaction temperature so that a higher percent of remelting will occur. Future research on amorphous steel will focus on both of these approaches in order to increase the hardness and the wear resistance of this new class of coatings.

## ACKNOWLEDGMENTS

The authors wish to thank Ames Laboratory for plasma spraying the steel coupons and Case New Holland for performing the three body wear tests. Research was supported through the

Defense Advanced Research Projects Agency (DARPA) under the DOE Idaho Operations Office Contract No. DE-AC07-99ID13727. This document has been approved for Public Release, Distribution Unlimited.

**REFERENCES**

- [1] T. Grosdidier, H.L. Liao, and A. Tidu, Thermal Spray Surface Engineering via Applied Research, Proceedings of the 1<sup>st</sup> International Thermal Spray Conference, May 8-11, 2000, 1341-1344.
- [2] M.L. Lau, E. Strock, A. Fabel, C.J. Lavernia, and E.J. Lavernia, *NanoStructured Materials*, 10(1998), 723-730.
- [3] V.L. Tellkamp, M.L. Lau, A. Fabel, and E.J. Lavernia, *NanoStructured Materials*, 9(1997), 489-492.
- [4] M.L. Lau, V.V. Gupta, and E.J. Lavernia, *NanoStructured Materials*, 12(1999), 319-322.
- [5] B.H. Kear and G. Skandan, *NanoStructured Materials*, 8(1997), 765-769.
- [6] H.G. Jiang, M.L. Lau, and E.J. Lavernia, *NanoStructured Materials*, 10(1998), 169-178.
- [7] M.L. Lau, V.V. Gupta, and E.J. Lavernia, *NanoStructured Materials*, 10(1998), 715-722.
- [8] Ying Chun Zhu and Chuan Xian Ding, *NanoStructured Materials*, 11(1999), 319-323.
- [9] J. Karthikeyan, C.C. Berndt, J. Tikkanen, J.Y. Wang, A.H. King, and H. Herman, *NanoStructured Materials*, 9(1997), 137-140.
- [10] J. Tikkanen, K.A. Gross, C.C. Berndt, V. Pitkänen, J. Keskinen, S. Raghu, M. Rajala, and J. Karthikeyan, *Surface and Coatings Technology*, 90(1997), 210-216.
- [11] N. P. Rao, H.J. Lee, M. Kelkar, D.J. Hansen, J.V.R. Heberlein, P.H. McMurry, and S.L. Girshick, *NanoStructured Materials*, 9(1997), 129-132.
- [12] Schmuel Eidelman and Xiaolong Yang, *NanoStructured Materials*, 9(1997), 79-84.
- [13] D.J. Branagan, Powder Metallurgy Alloys and Particulate Materials for Industrial Application, St. Louis, MO, 2000, ed. By David E. Alman and Joseph W. Newkirk, TMS, 111-122.
- [14] J.R. Weertman, D. Farkas, K. Hemker, H. Kung, M. Mayo, R. Mitra, and H. Van Swygenhoven, *MRS Bulletin*, Feb.(1999), 44-50.
- [15] R.S. Mishra, S.X. McFadden, R.Z. Valiev, and A.K. Mukherjee, *JOM*, January (1999), 37-40.
- [16] Kenneth C. Ludema, Friction, Wear, Lubrication; A Textbook in Tribology, CRC Press, New York, 1996, p149-151.
- [17] William L. Johnson, *MRS Bulletin*, Oct. (1999), 42-56.

**Table 1 Phase Information for the 750°C 1 Hour HVOF Coating**

Phase	Crystal System	Space Group	Lattice Parameters (Å)
$\alpha$ -Fe	Cubic	Im3m	a = 2.902
Fe <sub>23</sub> B <sub>6</sub>	Cubic	Fm3m	a = 10.615
Fe <sub>2</sub> B	Tetragonal	I4/mcm	a = 5.179, c = 4.229
Cr <sub>23</sub> C <sub>6</sub>	Cubic	Fm3m	a = 10.713

**Table 2 Results Of Rubber Wheel Wet Sand Slurry Tests**

Alloy	Hardness (GPa)	Avg. Weight Loss (g)

<b>As-Sprayed Steel</b>	<b>10.2</b>	<b>0.0795</b>
<b>Heat Treated Steel</b>	<b>11.4</b>	<b>0.0201</b>
<b>88% WC – 12% Co</b>	<b>12.8*</b>	<b>0.0082</b>

- \*Knoop hardness

## List of Figure Captions

- Figure 1 The wt% powder from sieving and the wt% glass from DSC measurements are shown as a function of sieved powder particle size.
- Figure 2 X-ray diffraction diagram for the as-atomized 10-20  $\mu\text{m}$  powder.
- Figure 3 Backscattered electron micrographs of the cross section of two as-atomized powder particles. A) 11  $\mu\text{m}$  particle with an amorphous structure B) 59  $\mu\text{m}$  particle with a primarily crystalline structure containing pockets of glass.
- Figure 4 Powder size distribution obtained after sieving the atomized powder less than 50  $\mu\text{m}$  followed by air classification.
- Figure 5 Example samples deposited by HVOF in air without a cover gas onto 4340 alloy steel, 13-8 stainless steel, and 7075 Al. The steel surfaces which were produced formed an amorphous structure.
- Figure 6 Cross sections of HVOF deposited as-sprayed steel coatings; A) Initial spraying, B) After optimization.
- Figure 7 X-ray diffraction scan of the free surface of a HVOF sprayed coating which was 330  $\mu\text{m}$  thick.
- Figure 8 X-ray diffraction scan of a plasma sprayed coating which was 1650  $\mu\text{m}$  in thickness; A) free surface, B) substrate surface.
- Figure 9 DTA scans of the air-classified powder, the as-deposited plasma coating, and the as-deposited HVOF coating.
- Figure 10 Experimental and Rietveld refined X-ray diffraction patterns of the heat treated (750°C for 1 hour) HVOF coating.
- Figure 11 TEM micrograph of the HVOF deposited alloy after a 750°C for 1 hour heat treatment.
- Figure 12 Profile curve of the wear 'groove' on the as-sprayed plasma deposited sample. After 2000 cycles of pin on disk testing, instead of the expected wear groove on the substrate, a hill of deposited  $\text{Si}_3\text{N}_4$  was found from the pin.
- Figure 13 Coefficient of friction versus the number of turns for Pin on Disk testing of the as-sprayed coating. Note that while the initial friction was low,  $\text{Si}_3\text{N}_4$  deposition and buildup caused the measured friction to increase to the  $\text{Si}_3\text{N}_4/\text{Si}_3\text{N}_4$  value.

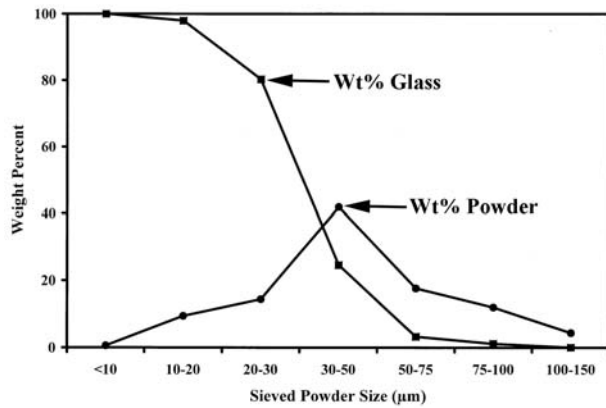


Figure 1 The wt% powder from sieving and the wt% glass from DSC measurements are shown as a function of sieved powder particle size.

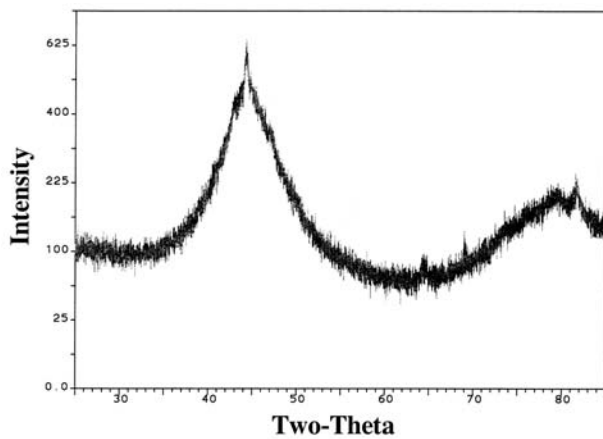


Figure 2 X-ray diffraction diagram for the as-atomized 10-20 μm powder.

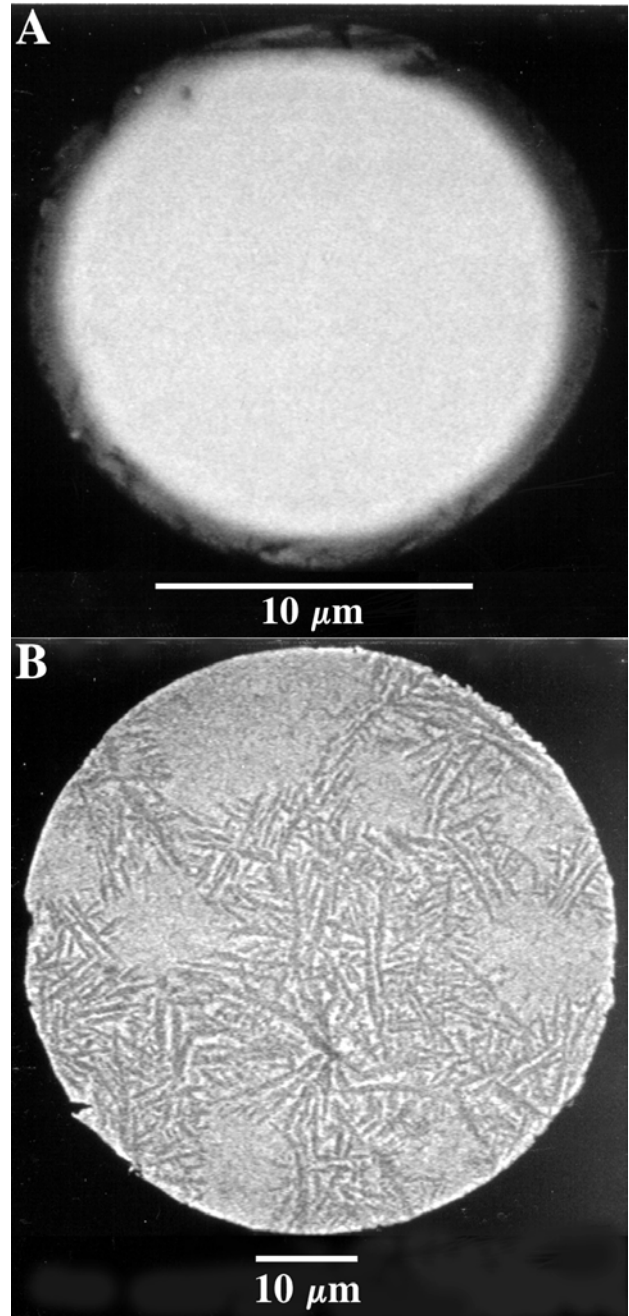


Figure 3 Backscattered electron micrographs of the cross section of two as-atomized powder particles. A) 11 μm particle with an amorphous structure B) 59 μm particle with a primarily crystalline structure containing pockets of glass.

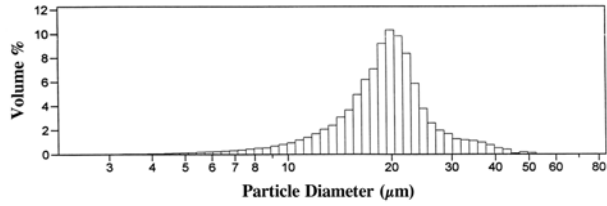


Figure 4 Powder size distribution obtained after sieving the atomized powder less than 50  $\mu\text{m}$  followed by air classification.

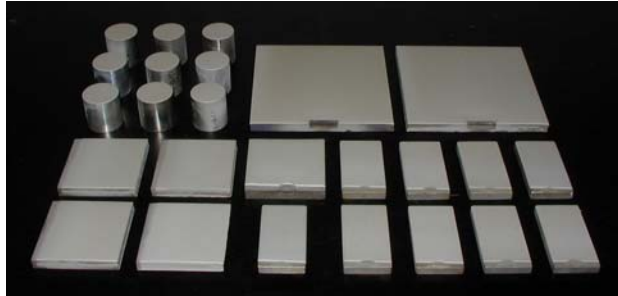


Figure 5 Example samples deposited by HVOF in air without a cover gas onto 4340 alloy steel, 13-8 stainless steel, and 7075 Al. The steel surfaces which were produced formed an amorphous structure.

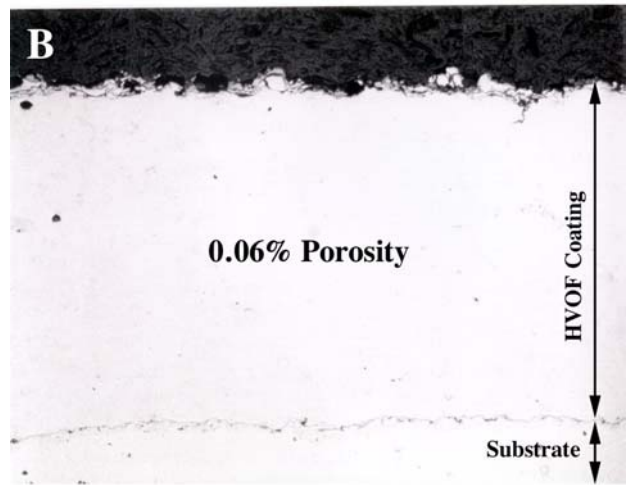
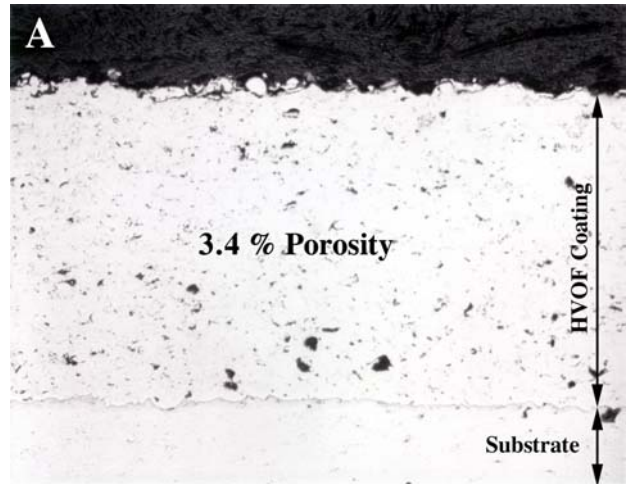


Figure 6 Cross sections of HVOF deposited as-sprayed steel coatings; A) Initial spraying, B) After optimization.

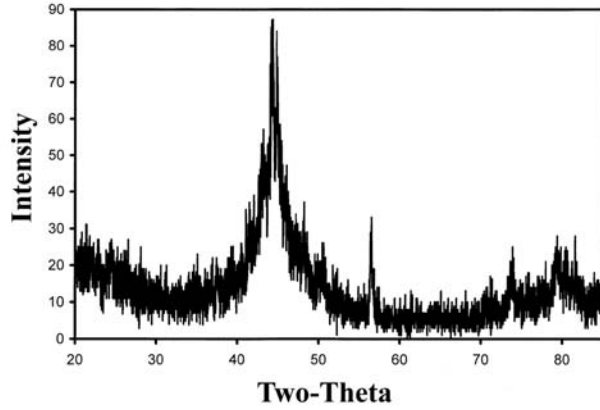


Figure 7 X-ray diffraction scan of the free surface of a HVOF sprayed coating which was 330  $\mu\text{m}$  thick.

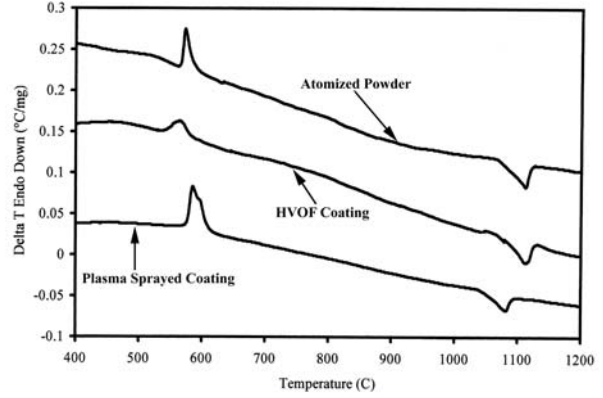


Figure 9 DTA scans of the air-classified powder, the as-deposited plasma coating, and the as-deposited HVOF coating.

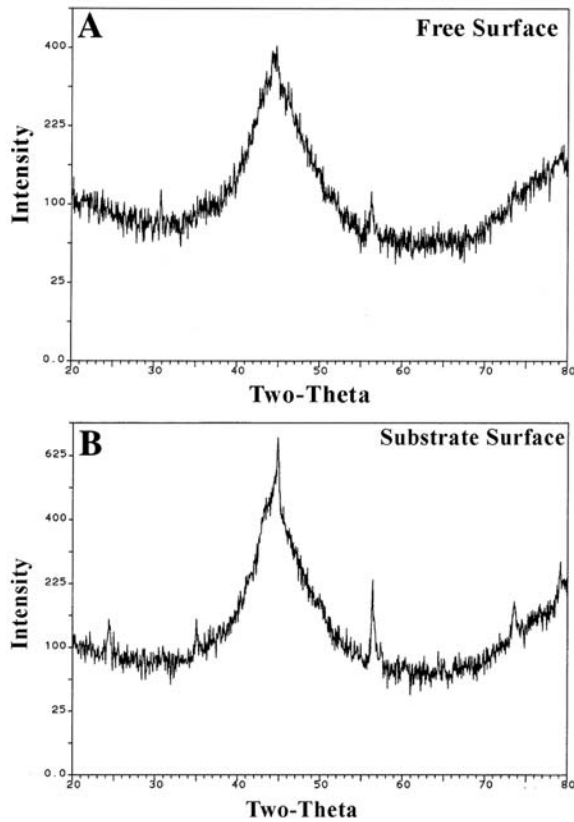


Figure 8 X-ray diffraction scan of a plasma sprayed coating which was 1650  $\mu\text{m}$  in thickness; A) free surface, B) substrate surface.

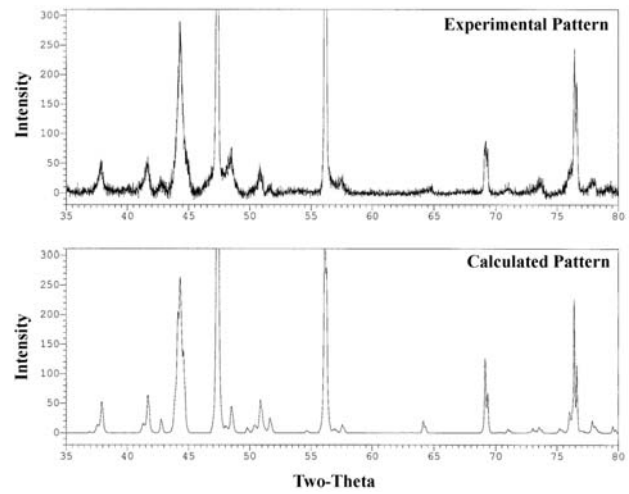


Figure 10 Experimental and Rietveld refined X-ray diffraction patterns of the heat treated (750 $^{\circ}\text{C}$  for 1 hour) HVOF coating.

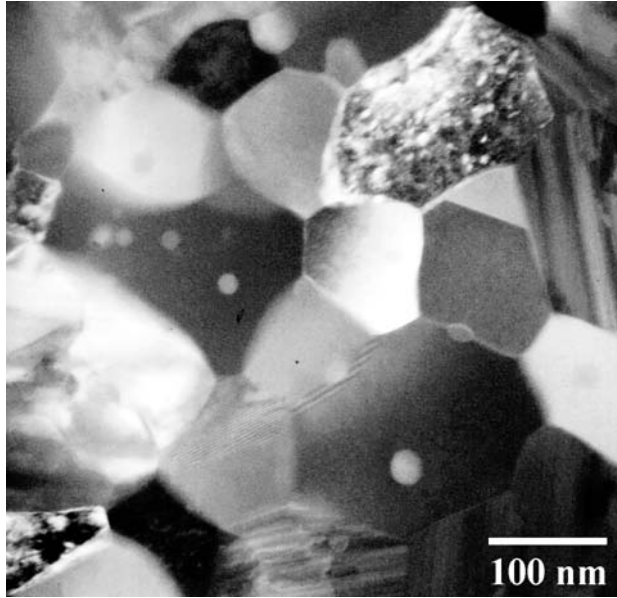


Figure 11 TEM micrograph of the HVOF deposited alloy after a 750°C for 1 hour heat treatment.

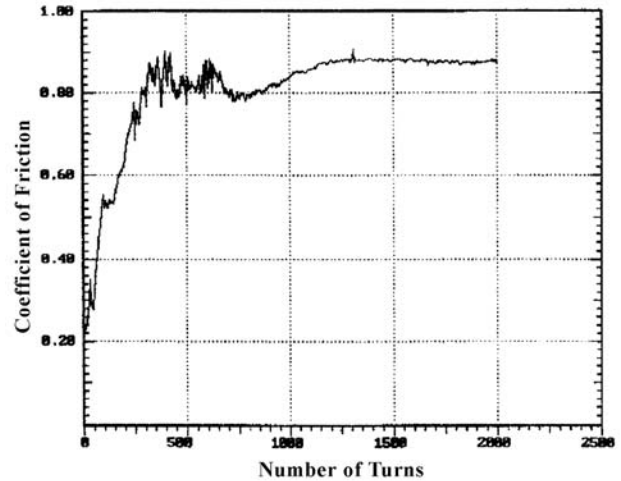


Figure 13 Coefficient of friction versus the number of turns for Pin on Disk testing of the as-sprayed coating. Note that while the initial friction was low,  $\text{Si}_3\text{N}_4$  deposition and buildup caused the measured friction to increase to the  $\text{Si}_3\text{N}_4/\text{Si}_3\text{N}_4$  value.

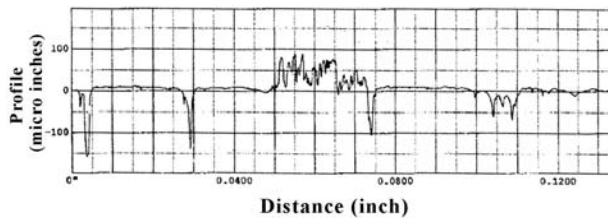


Figure 12 Profile curve of the wear 'groove' on the as-sprayed plasma deposited sample. After 2000 cycles of pin on disk testing, instead of the expected wear groove on the substrate, a hill of deposited  $\text{Si}_3\text{N}_4$  was found from the pin.